



HAL
open science

Dual-Band Circularly Polarized Transmitarray Antenna for Satellite Communications at (20 to 30) GHz

Hamed Hasani, Joana S. Silva, Santiago Capdevila, Maria Garcia-Vigueras,
Juan R. Mosig

► **To cite this version:**

Hamed Hasani, Joana S. Silva, Santiago Capdevila, Maria Garcia-Vigueras, Juan R. Mosig. Dual-Band Circularly Polarized Transmitarray Antenna for Satellite Communications at (20 to 30) GHz. IEEE Transactions on Antennas and Propagation, 2019, 67 (8), pp.5325-5333. 10.1109/TAP.2019.2912495 . hal-02277964

HAL Id: hal-02277964

<https://univ-rennes.hal.science/hal-02277964>

Submitted on 9 Sep 2019

HAL is a multi-disciplinary open access archive for the deposit and dissemination of scientific research documents, whether they are published or not. The documents may come from teaching and research institutions in France or abroad, or from public or private research centers.

L'archive ouverte pluridisciplinaire **HAL**, est destinée au dépôt et à la diffusion de documents scientifiques de niveau recherche, publiés ou non, émanant des établissements d'enseignement et de recherche français ou étrangers, des laboratoires publics ou privés.

Dual-band Circularly Polarized Transmitarray Antenna for Satellite Communications at 20/30 GHz

Hamed Hasani, Joana S. Silva, Santiago Capdevila, María García-Vigueras, and Juan R. Mosig

Abstract— A novel dual-band polarization-independent transmitarray is introduced in this paper for communication systems in Ka band. Thanks to its unit-cell topology, the transmitarray antenna demonstrates almost complete independent performance at the two design frequency bands of 20 and 30 GHz. As a proof-of-concept, a transmitarray antenna prototype having a plate size of 80×80 mm² has been fabricated using printed board technology. A dual-band circularly polarized ridged cavity antenna feeds this planar structure and the relative translational displacement between the feed and the transmitarray allows beam steering. The antenna performance has been validated via experimental results, which demonstrate good agreement with the theoretical and simulation predictions carried out with commercial software packages.

Index Terms— Transmitarray, dual-band, circular polarization, beam-steering, millimeter wave, satellite communications, Ka band, cavity-backed feed antenna.

I. INTRODUCTION

IN the recent years, satellite communication systems operating in Ka band (downlink: 17-21.2 GHz; uplink: 27.5-31 GHz) [1] have attracted great attention mainly due to the spot-beam coverage allowing frequency reuse operation and consequently higher capacity. Moreover, operation in higher frequencies allow considerable size reduction, which *per se* has boosted the interest on satellite-on-the-move applications (SOTM) guaranteeing an always-connected nomadic behavior. Transmitarrays antennas have proven to be reliable candidates (as high-gain, low-profile and low-cost antennas) for multiple applications, especially those of satellite communications systems.

H. Hasani formerly with Laboratoire d'Electromagnétisme et d'Antennes, École Polytechnique Fédérale de Lausanne, Lausanne 1015, Switzerland, and currently with Sivantos GmbH, Henri-Dunant Str. 100, 91058 Erlangen, Germany (hamed.hasani@sivantos.com).

J. S. Silva is with Laboratoire d'Electromagnétisme et d'Antennes, École Polytechnique Fédérale de Lausanne, Lausanne 1015, Switzerland, and currently with HUBER+SUHNER AG.

S. Capdevila is with Laboratoire d'Electromagnétisme et d'Antennes, École Polytechnique Fédérale de Lausanne, Lausanne 1015, Switzerland.

M. Garcia-Vigueras is with Institut d'Électronique et de Télécommunications de Rennes, UMR CNRS 6164, Institut National des Sciences Appliquées de Rennes, Rennes 35708, France.

J. R. Mosig formerly with Laboratoire d'Electromagnétisme et d'Antennes, École Polytechnique Fédérale de Lausanne, Lausanne 1015, Switzerland.

A transmitarray antenna [2] consists of a flat surface illuminated by a feed antenna. The flat surface comprises an array of multi-layer printed structures each with a different geometrical parameter that controls the transmission amplitude and phase of the incoming wave. The phase control capability should allow the array to transform the incoming spherical wave front into plane wave hence generating a highly directive beam in the far-field region

In the literature, several multi-band transmitarrays have been described [3-11]. In [3] a printed dual-band transmitarray at 20/30 GHz is introduced which uses interlaced cross-dipoles printed on four layers. An active transmitarray for similar purposes is presented in [4] for beam direction at broadside which uses dual-band subarrays. A dual-band transmitarray is introduced in [5] performing at around 12 and 17 GHz with linear polarization at each frequency. In [6] and [7] cell topologies are proposed for dual-band performance controlling the transmission phase through element rotations and hence restricting the operation to circular polarization only. As for metallic transmitarrays a dual-polarized cell topology has been recently introduced in [8] but for closely spaced frequencies of 11 and 12.5 GHz. A recent concept is introduced in [9] for dual-band, dual-polarized performance at 20/30 GHz. The transmitarray is composed of seven layers each composed of an array of printed cross dipoles and square rectangular apertures. In addition, beam steering functionality is achieved through the relative positioning of feed vs transmitarray surface. In the design process, the phase response of the proposed cell at each frequency is a function of the size of each element and thus a time-consuming cell optimization process has been carried out in order to obtain the optimum transmission amplitude/phase. Furthermore, the usage of dielectrics is unavoidable which makes the antenna suitable only for ground terminals.

This paper presents a cell topology for dual-band dual-polarized performance at 20 and 30 GHz which, compared to the above-mentioned solutions, possesses additional distinctive advantages. The proposed cell demonstrates independent performance at each frequency band which eliminates the need for time-consuming phase optimization techniques and brings flexibility since the antenna can be designed to have arbitrary beam direction at each frequency band. Furthermore, due to the dual-polarized structure of the cell, it can be employed for any polarization (e.g.: circular, linear, slant).

In addition to the above-mentioned cases, the cell has the potential to be developed as a fully metallic topology which can be an attractive solution for space environments. The main challenge encountered in this case is the cell miniaturization in

order to avoid grating lobes at 30 GHz. This difficulty stems from the relatively large difference in the design frequencies and it is discussed in detail in this paper.

The paper is organized as follows. The unit-cell topology is presented in section II. The antenna design along with a simulation scenario is described in Section III. Section IV presents the simulated and measured beam steering results based on the concept used in [10]. The possibility of an extension to a fully metallic transmitarray is presented in section V along with simulation results. Finally, conclusions are drawn in Section VI.

II. THE UNIT-CELL

The unit-cell geometry along with the assigned input and output Floquet ports, are shown in Fig. 1. The remaining four surrounding walls are assigned with periodic boundary condition (PBC). The cell is composed of three layers, each being composed of interlaced dual-polarized slot elements for phase regulation at 20 and 30 GHz. The phase regulating parameters are denoted as $L1$ (for 20 GHz) and $L2$ (for 30 GHz). The cell is thus capable of operation for elliptical polarization in general and in particular for linear, circular and slant polarizations. While a simple cross-slot element has been chosen for operation at 30 GHz, a swastika cross is designated for operation at 20 GHz for miniaturization purposes to maintain the cell size no larger than 5.3 mm. This cell size should allow beam deviation up to 60 degrees from the broad side direction at 30 GHz without the appearance of grating lobes. Furthermore, as will be discussed in detail in section V, a swastika cross proves to be an excellent candidate for the design of the fully metallic dual-band transmitarray antenna. We should also note that according to [12] the cell is a Rot-4 type topology; a topology whose amplitude and phase response is invariant to a physical 90 degrees rotation around z axis (assuming z axis normal to the paper in Fig. 1a). This topology in theory demonstrates zero cross-polarization level in case of a normal wave incidence.

The slot elements are designed to be printed on Rogers-5870 with 0.254 mm of thickness and permittivity 2.33. Layers are separated by air gaps of fixed thickness $h = 3.6$ mm, which makes the total array thickness of around 7.5 mm. In the current dual-band design we have chosen the value of 3.6 mm as layer separation distance due to the availability of an antenna support which was previously designed and fabricated for similar purposes. Furthermore, as will be shown later, the chosen value is adequate for proof-of-concept purposes.

Fig. 2 shows the cell amplitude and phase response at each frequency with respect to their own corresponding phase regulating parameter i.e. $L1$ or $L2$. At 20 GHz, the cell demonstrates around 300° phase range within the 3-dB range for transmission power $|S_{12}|^2$. At 30 GHz however return loss has increased for certain values of $L2$ within the 3dB transmission power range. The cell performs better at 20 GHz, where the 3.6 mm layer separation is closer to a quarter wavelength at 20 GHz ($\lambda_{20}/4 = 3.75$ mm) than at 30 GHz ($\lambda_{30}/4 = 2.5$ mm). This effect is better shown in Fig. 3, where simulated cell transmission and reflection magnitudes are obtained in terms of *frequency* for different values of layer

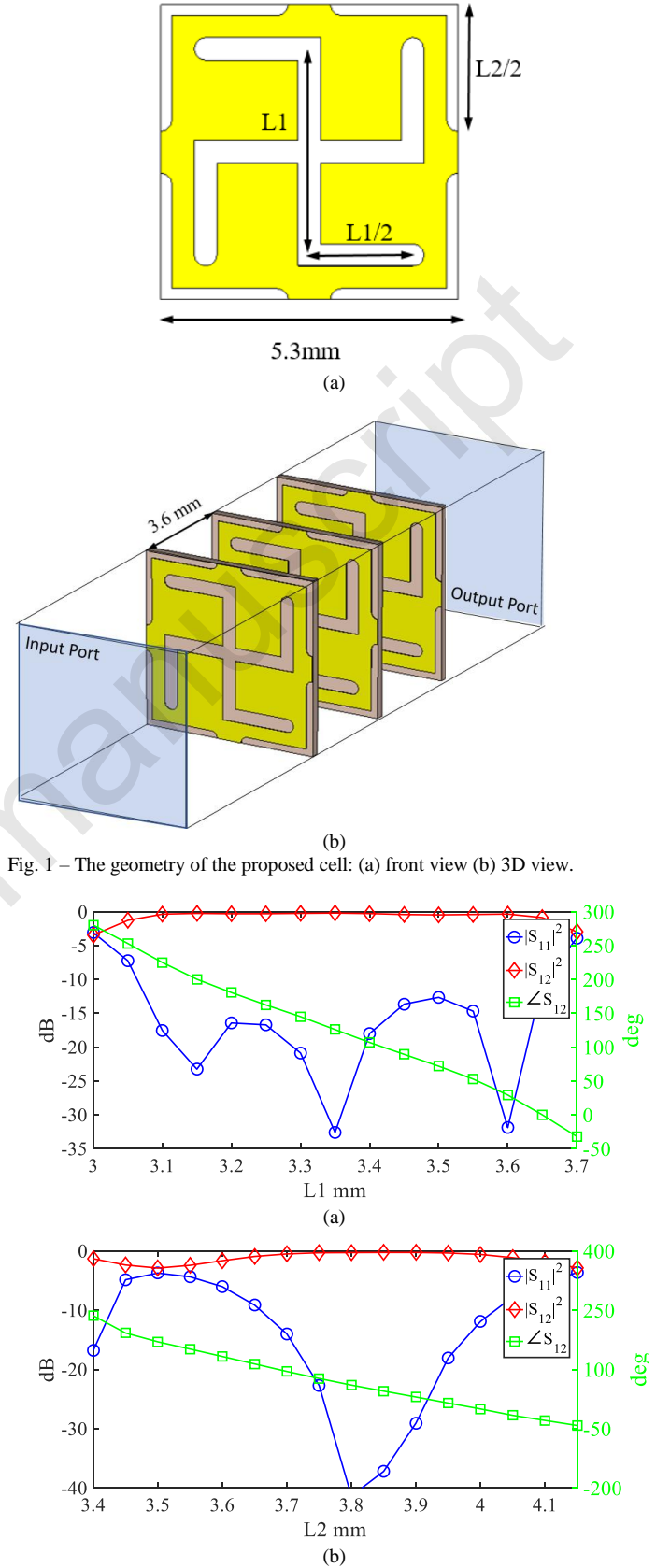


Fig. 1 – The geometry of the proposed cell: (a) front view (b) 3D view.

Fig. 2 – Phase and amplitude response of the cell: (a) at 20 GHz with respect to $L1$; (b) at 30 GHz with respect to $L2$.

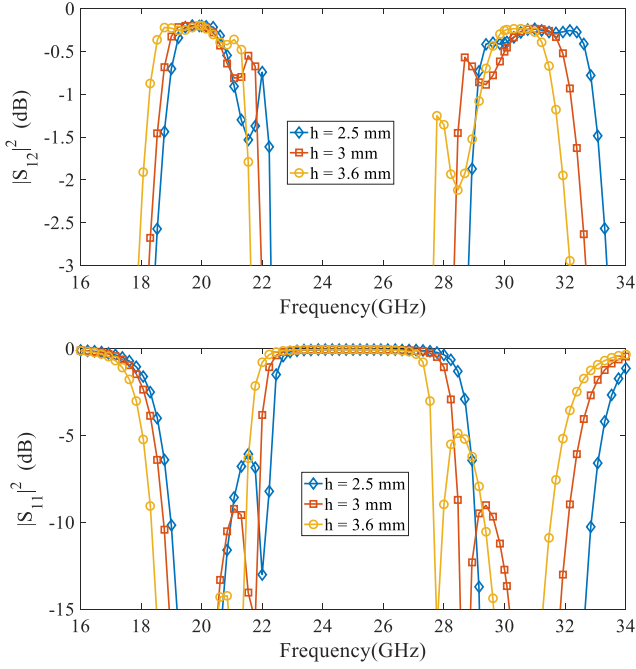


Fig. 3. Cell frequency response for transmission and reflection power for different values of layer separation.

separation at resonant values of $L1 = 3.35$ mm and $L2 = 3.75$ mm.

As shown, for a layer distance of 2.5 mm the performance is best at 30 GHz, where this quarter wavelength distance results in a flat transmission power across the bandwidth. At 20 GHz, however, transmission drop will be produced at the higher end of the bandwidth. As the layer separation is increased to an intermediate value of 3 mm, drops occur at both frequencies in the extremities of the transmission response. However, the performance remains acceptable since reflection coefficient is kept below -10dB within the cell bandwidth. Further increase in layer separation to the current value of 3.6 mm, enhances the performance at 20 GHz while imposing a negative effect at 30 GHz.

The interested reader is referred to [13], where a thorough study on the layer separation effect and maximum achievable phase range of periodic structures intended for transmitarray design has been carried out.

In Fig. 4, the response of the cell at each frequency has been simulated in CST [14] against variations of the parameters directly linked to that frequency ($L1$ for 20 GHz, $L2$ for 30 GHz). One of the main advantages of the cell proposed in this paper is now evidenced here. As shown in Fig. 4a, at 20 GHz the phase response is only a function of $L1$ and the variation of $L2$ has almost no influence. The reciprocal is visible in Fig. 4b at 30 GHz. These results can in fact be interpreted as having two independent and uncoupled single-band transmitarrays sharing the same surface.

One of the factors that should also be considered is the cell phase and amplitude sensitivity to the angle of incidence. To this end, the cell response, at both 20 and 30 GHz has been obtained for several oblique wave incidences for a circularly polarized impinging wave. As shown in Fig. 5a, at 20 GHz the cell phase response is resilient to the simulated angles of incidence. There occurs however a drop in the cell

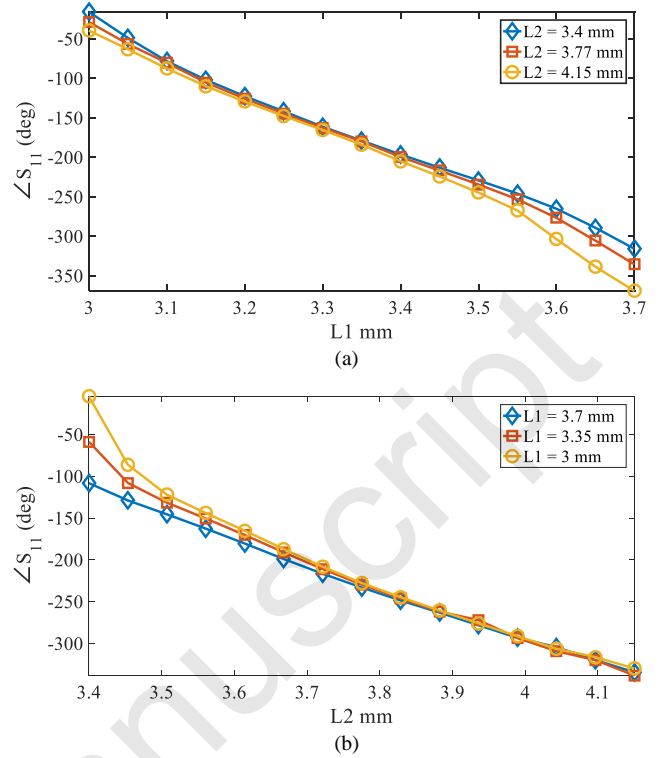


Fig. 4 - Phase responses: a) at 20 GHz; b) at 30 GHz. Please note that the variation of phase regulation parameter at one frequency has almost no effect on the phase response at the other frequency.

transmission response for $L1$ values around 3.35 mm (Fig. 5b). As the angle of incidence increases, this reduction becomes more noticeable reaching values of -3 dB at ($\theta = 30^\circ$, $\phi = 45^\circ$, $L1 = 3.3$ mm). Furthermore, as shown in Fig. 5c, level of cross-pol increases as well for all values of $L1$. Note that the broadside cross-pol level is not shown, as it remains below -40 dB.

To better understand this issue, Fig. 6 shows the cell frequency response for different incident angles at the resonant value of $L1 (= 3.35$ mm). As shown, for higher incident angles a magnitude drop in transmission response occurs which increases with the angle of incident reaching to the maximum value of 6 dB. The main reason is that under these conditions, the cell is transparent to TM waves while it blocks the TE waves, which results in the expected drop value of 6 dB for a circularly polarized impinging wave. The consequence of this behavior is that, certain cells on the transmitarray will exhibit sensitive transmission values depending on their perceived angle of incidence from the feed and on their phase regulating parameter value (here $L1$). This phenomenon will also result in somewhat higher scan losses.

Corresponding results for incident angle sensitivity at 30 GHz are shown in Fig. 7. Here the transmission phase response shows low levels of deviation (maximum 50°) at oblique incident angles while the transmission amplitude response shows deviations at low values of $L2$ (see Fig. 7b). This is mainly due to the layer electrical distance at 30 GHz as evidenced in Fig. 3. Cross-pol level, shown in Fig. 7c, similar to 20 GHz, increases for all values of $L2$ at oblique incident angles especially when $\phi = 45^\circ$.

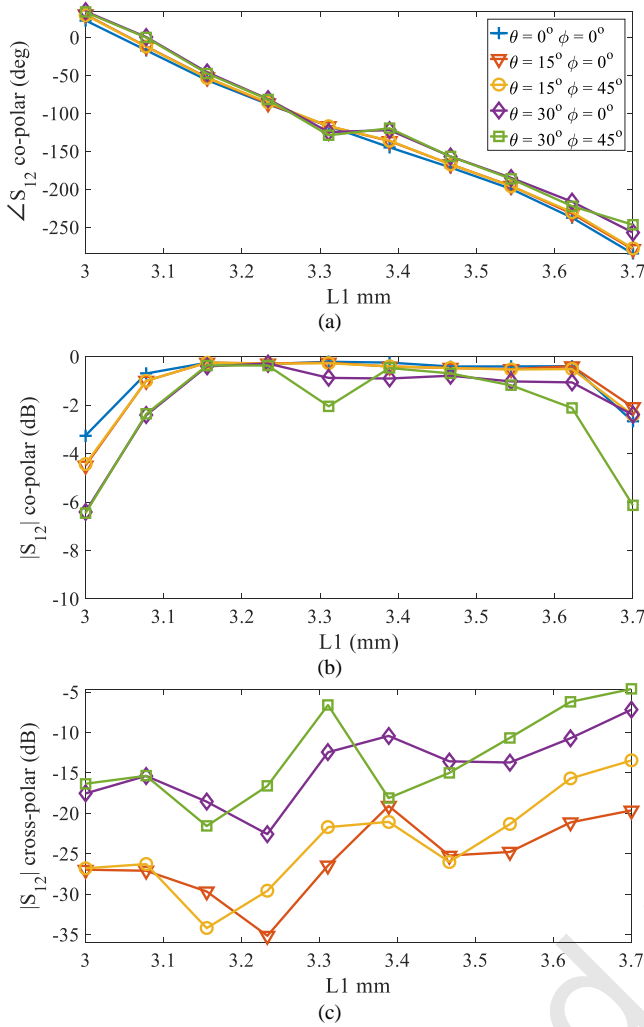


Fig. 5 - At 20GHz for circular-polarization. Cell amplitude and phase response for several oblique waves with incidence angle (θ, ϕ).

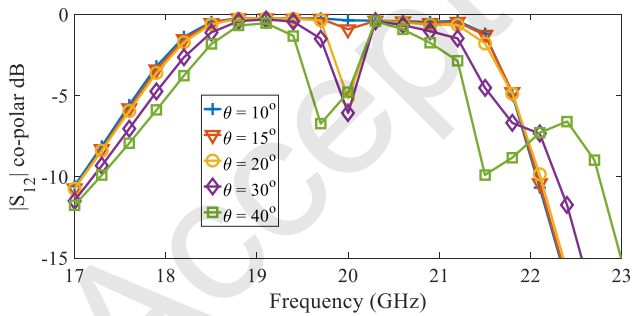


Fig. 6 - Cell transmission response versus frequency around 20 GHz for several oblique waves with incidence angle ($\theta, \phi = 45^\circ$) for circularly polarized wave. L1 and L2 are kept at their resonant values: 3.35 mm and 3.7 mm, respectively.

III. ANTENNA DESIGN

A. Transmitarray

The following design considers a proof-of-concept transmitarray with an aperture size of $80 \times 80 \text{ mm}^2$ fed by a dual-band circularly polarized ridged cavity slot antenna. The transmitarray is in fact comprised of two superimposed arrays

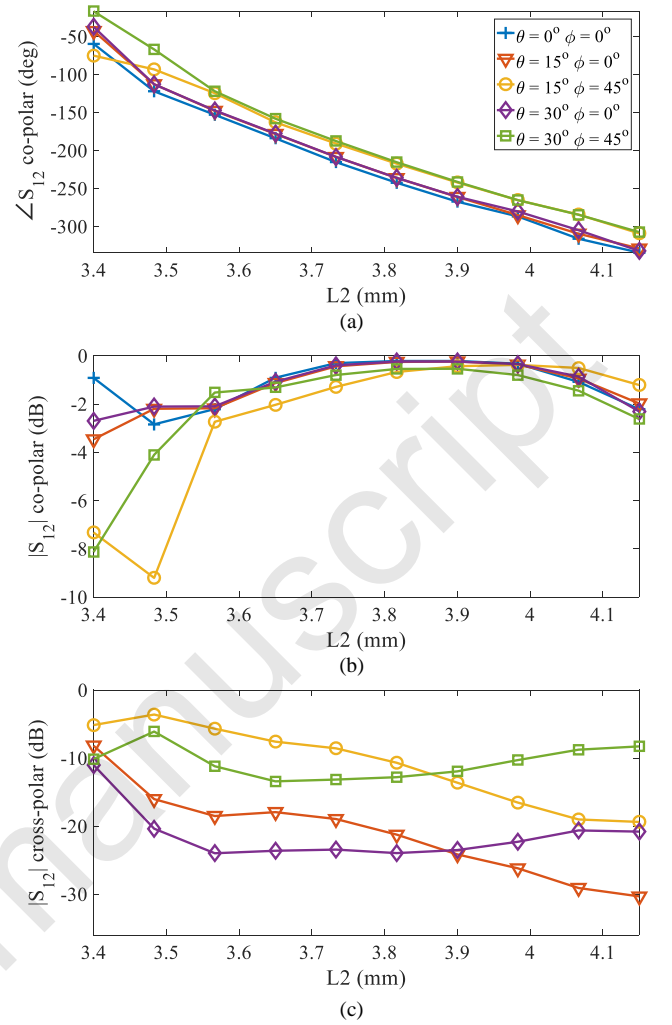


Fig. 7 - At 30GHz for circular-polarization. Cell amplitude and phase response for several oblique waves with incidence angle (θ, ϕ).

with 14×14 and 13×13 elements for 20 and 30 GHz, respectively. The first design step consists in determining the optimum focal point. This can be estimated by considering the pattern of the feed antenna and the array size. If the feed antenna has different radiation patterns and directivities at each frequency band, a different value for the optimum focal point should be considered at each frequency. Instead, in the current work and for the sake of technological simplicity, we chose to work with the average of the feed radiation patterns at both frequencies, thus yielding a unique value of 55mm for the optimum focal point. With this value, the angle of incidence at the array edge becomes 35° and the illumination taper becomes -5.1 dB and -7.2 dB on the array edge, and -8 dB and -12 dB on the array corners at 20 and 30GHz, respectively. As expected, the tapering tends to follow the feed different directivities at each frequency, but this can be always compensated.

The overall structure was then simulated in FEKO [15] due to the unique features offered by the software which facilitates the simulation in terms of time and computation load while maintaining enough accuracy. In the simulation process, which uses integral equation formulation, the transmitarray is treated as a multi-layer structure with all the layers

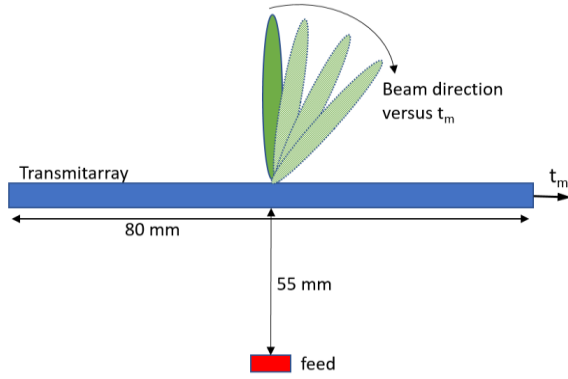


Fig. 8 - Schematic presentation of beam scanning by lateral translation (t_m) of the transmitarray.

(PEC+substrate) extended to infinity. The slot elements are then placed on the metallic layers and are assigned as apertures by the solver. With this arrangement, only the slot apertures are meshed, and the solver uses embedded Green's functions for multilayer planar structures to compute the fields.

The whole structure is then illuminated by a point source placed at 55 mm beneath the structure which has the individual radiation pattern of the ridged cavity slot antenna at each frequency. An important remark is that since the simulation considers an infinite PEC ground plane, diffraction from the transmitarray edges, in addition to metallic losses, will not be considered.

B. Cavity-backed feed antenna

The feed antenna has been described in [16-17]. It can be viewed as a cylindrical cavity loaded with eight ridges, which are responsible for the dual-band operation, covering the entire downlink and uplink Ka bands. The top wall of the cavity is a metallic circular lid with a crossed slot. The sequential rotation feeding implemented through four coaxial cables requires successive 90° phase shifts to produce circular polarization (CP). A dedicated dual-layer beam-forming network (BFN) comprising two microstrip circuits, each one with an input port associated to one frequency, provides this phase difference, allowing right-hand CP radiation at 20 GHz and left-hand CP at 30 GHz.

At both 20 GHz and 30 GHz, the insertion losses associated to the BFN are lower than 1.6 dB. The complete feed antenna presents a reflection coefficient below -24 dB and the isolation between the two input ports is below -20 dB at both frequencies.

The antenna (including BFN) presents a measured gain of 5 dBi and half power beam width of 70° and 50° at 20 GHz and 30 GHz, respectively. The beam steering was achieved by displacing the Tx-array laterally from the reference position (i.e. when both Tx-array and feed antenna are aligned) with steps of 10 mm until a maximum of 30 mm (see Fig. 8 for a schematic presentation). The simulated radiation patterns at 20 GHz and 30 GHz are presented in Fig. 9. As shown, beam scanning is achieved up to 24 degrees by mechanically displacing the array with respect to the feed. The basic electromagnetic mechanism behind this technique is elaborated in [10]. The simulated performance indicators for

both frequencies are summarized in Table I, where t_m is the translational movement of the Tx-array, α_{beam} is the beam tilt angle, G is the gain and ΔG is the scan loss. The scan losses, as indicated in Table I, are caused by low aperture efficiency and a non-linear phase profile on the array surface due to an off-set illumination. In addition, scan loss is directly related to the unit-cell radiation pattern (here we consider a dual-linear polarized slot on an infinite ground plane). It can be shown that at both frequencies pure RHCP or LHCP normalized power radiation pattern can well be approximated by $(\frac{1+\cos\theta}{2})^2$, where θ is the scan angle.

According to the simulation results, the antenna demonstrates total aperture efficiency of 20% and 15% at 20 and 30 GHz respectively. These values are obtained by dividing antenna gain by the directivity achieved from a uniformly illuminated surface with an area equal to that of the transmitarray.

One should however note that with the current feed pattern, in theory a maximum of 60% aperture efficiency (which is the multiplication of illumination and spillover efficiencies) is obtainable. In addition, efficiency is further reduced due to the transmission amplitude of cells (see Fig. 2). To this end, cell efficiency has been estimated by averaging the transmission coefficient (i.e. $|S_{12}|^2$) of all the cells, reaching values around 70% and 65% at 20 and 30 GHz, respectively. As a result, the total estimated efficiency is obtained as follows:

$$\eta_T = \eta_i \times \eta_s \times \eta_{cell} \times \eta_{feed} \quad (1)$$

Where η_i is the illumination efficiency, η_s the spillover efficiency, η_{cell} the cell efficiency and η_{feed} is the feed efficiency (which in simulation is considered to be 100%). The estimated value of total efficiency for 20 and 30 GHz is thus 42% and 39%, respectively. However, there are other factors that reduce the total efficiency:

The small dimension of the array has a negative effect since the proximity of array edges perturbs the elements' expected amplitude and phase which were originally computed in a periodic environment. Other factor is the radiation energy leakage into the cross-polar component radiated from the feed as one moves away from its broadside direction. Furthermore, according to Figs. 5-7 cross-pol level increases and losses occur at oblique incident angles. These factors are believed to have caused total efficiency to be reduced to the final simulated values of 20% and 15% at 20 and 30 GHz, respectively (see Table III).

IV. EXPERIMENTAL RESULTS

In order to validate the previous theoretical results, the Tx-array was manufactured using standard photolithographic techniques for printed circuit board. Rohacell frames ($\epsilon_r \sim 1.05$, $\tan\delta \sim 0.01$ @ 26.5 GHz) were used to keep the layers at the proper distance, and the complete "tri-layer" structure was introduced in a 3D-printed support. The support was able to hold the three different layers at 3.6 mm and had the capability for lateral displacement of the transmitarray to enable the steering of the beam, while also holding the feed antenna at the desired distance, as shown in Fig. 10.

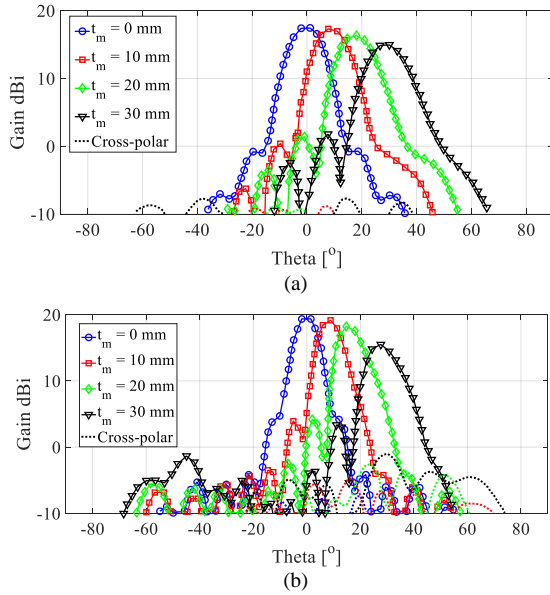


Fig. 9 - Simulated radiation patterns for different positions of the Tx-array ($0 \text{ mm} < t_m < 30 \text{ mm}$, with steps of 10 mm): (a) at 20 GHz; (b) at 30 GHz.

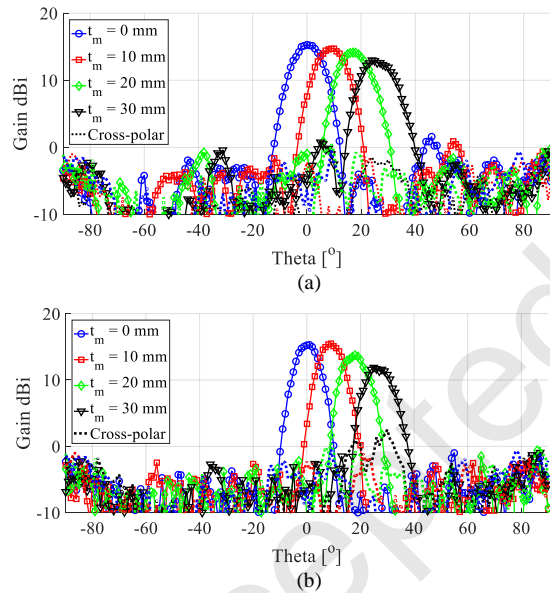


Fig. 11 – Measured circular-polarized radiation patterns for different positions of the Tx-array ($0 \text{ mm} < t_m < 30 \text{ mm}$, with steps of 10 mm): (a) at 20 GHz; (b) at 30 GHz.

As mentioned in section III, the simulations were carried out with special conditions to reduce simulation time and memory requirements, which implied among other, the use of infinite ground planes. Since such conditions cannot be realized, in the real case the dimensions of the transmitarray are of $80 \times 80 \text{ mm}^2$, and thus, non-idealities such as metallic losses in copper, the diffraction from the edges of the transmitarray and the presence of the antenna support will have a negative effect on the measured gain, even if we try to minimize them with absorbers.

The full transmitarray antenna was mounted in the anechoic chamber at EPFL and a ridged horn antenna, which provides

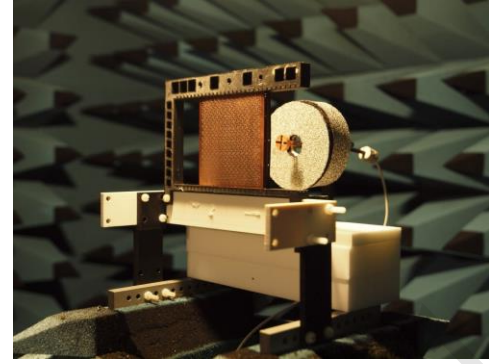


Fig. 10 - Fabricated prototype.

TABLE I.
SIMULATION RESULTS SUMMARY

t_m [mm]	20 GHz			30 GHz		
	α_{beam} [°]	G [dBi]	ΔG [dB]	α_{beam} [°]	G [dBi]	ΔG [dB]
0	0	18	0	0	19.6	0
10	9	17.7	0.3	9	19.1	0.5
20	18	16.7	1.3	17	17.7	1.9
30	26	15	3	26	15.4	4.2

TABLE II.
MEASUREMENT RESULTS SUMMARY

t_m [mm]	20 GHz			30 GHz		
	α_{beam} [°]	G [dBi]	ΔG [dB]	α_{beam} [°]	G [dBi]	ΔG [dB]
0	0	15.3	0	0	15.3	0.2
10	10	14.7	0.6	9	15.5	0
20	18	14.1	1.2	18	13.7	1.8
30	24	13	2.3	25	11.9	3.6

linear polarization over the whole frequency range of interest, was used as the probe antenna placed at the transmitarray antenna far-field. In order to fully characterize the antenna, a rotation of 90° of the probe antenna is done for each point of measurement to obtain two orthogonal linear polarizations. The measurements were limited to the elevation plane of steering due to limitations of the anechoic chamber. Finally, the gain was characterized for the broadside configuration by comparison using two standard gain horn antennas at 20 GHz and 30 GHz.

A set of measurements were performed where the transmitarray was laterally moved within the 3D-printed support in steps of 10 mm, to achieve up to almost 30° of the positions are presented in Fig. 11 and the measured beam steering in elevation. The measurement results for all performance indicators for both frequencies are summarized in Table II. By comparing Table I and Table II, we can see that there is a difference in gain of 2.7 dB at 20 GHz and 4.3 dB at 30 GHz in broadside direction. This can be justified by the different scenarios considered in simulation and measurement. The most important factor is the efficiency of the feed, since in the simulation array is fed with a feed having 100% efficiency (due to the employment of lossless materials) whereas in practice it is around 50% at 20 and 30 GHz.

TABLE III.
APERTURE EFFICIENCY

	Efficiency	Simulation	Measurement
	20 GHz	Illumination× Spillover	60%
Feed		100%	50%
Cell		70%	70%
Estimated		42%	21%
Obtained from simulation/measurement		20%	10%
30 GHz	Illumination× Spillover	60%	60%
	Feed	100%	50%
	Cell	65%	65%
	Estimated	39%	19.5%
	Obtained from simulation/measurement	15%	6%

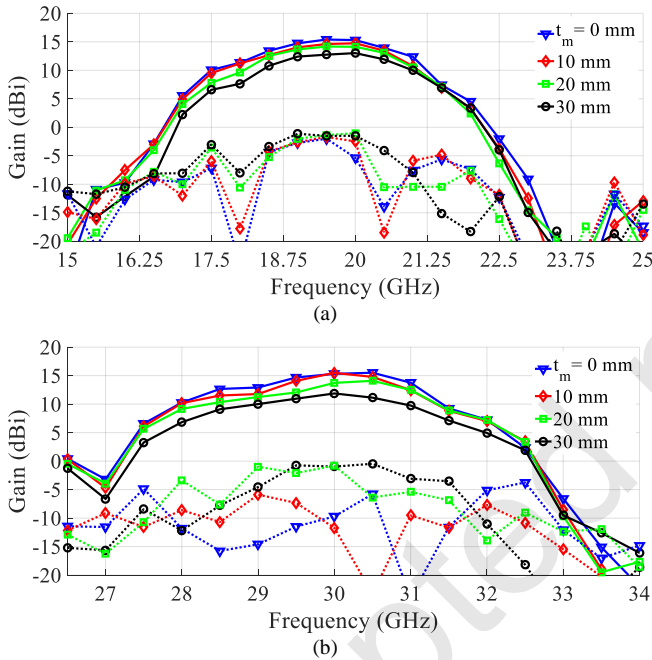


Fig. 12 - Co- and cross-polar gain, shown respectively by solid and dashed line, versus frequency at the corresponding scan angle.

Table III provides a summary on the estimation of array efficiency. It should be noted that for illumination, spillover and cell efficiencies we assumed the same values in simulation and measurement. Beside the mentioned factors, edge diffraction, fabrication tolerance and conductor losses in the transmitarray also have their own negative effect on the gain. The influence of these factors is more severe at 30 GHz. Measured co- and cross- polar gain versus frequency can be seen in Fig. 12. Gain has also been measured at the angles denoted by α_{beam} in Table II for four corresponding values of t_m . As shown the transmitarray has approximately 3-dB bandwidth of 10% and 7% around 20 and 30 GHz which translates into 2 GHz bandwidth at each frequency.

V. EXTENSION TO FULLY METALLIC IMPLEMENTATION

This section is dedicated to present a *qualitative* elaboration on the potential advantage of the proposed cell topology in that, by slight cell modification, it can be used to readily design a fully metallic transmitarray antenna. In fact, the cell topology explained so far is a special case of the following structure.

For a fully metallic cell, the main challenge is the slot length. This is of notable importance since the absence of any dielectric calls for longer slots which in turn requires a larger cell size and ultimately limits the array maximum beam deviation due to the grating lobes.

The solution to this issue is best shown in Fig. 13 where for both frequencies, interwoven swastika crosses are employed.

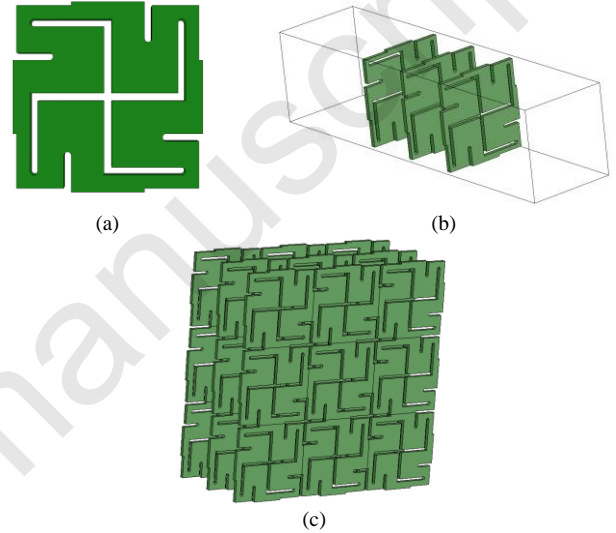


Fig. 13 - The geometry of the proposed dual-band cell for construction of fully metallic transmitarray.

As shown, due to the special geometry of the elements, they can be implemented on the same surface without any physical interference. In this structure, the layer separation is 3.6 mm with stainless steel (or in general any good electrical conductor) with 0.6 mm of thickness. Cell size is designated as 5mm. For brevity purposes, we demonstrate here only the full-wave simulation results carried out in Ansys HFSS [18] to show the capability of the resultant array. Furthermore, in order to save time and resources, the array is designed with 24 cells in one direction and periodic in the other direction, giving rise to the final structure shown in Fig. 14. To make the design more realistic a metallic pin at one extremity of the array connects all the layers together to keep them at the desired separation. The array is then fed by a Floquet port through the bottom surface with fundamental mode TE₀₀ while the upper surface is assigned as radiation boundary.

The array is thus designed to deflect a normally incident linearly polarized plane wave to 30 degrees off broadside direction at both 20 and 30 GHz. It is important to mention that the number of cells in the array and the deflection angle are chosen such that the required phase profile at both frequencies become periodic both with a common periodicity which corresponds to the array length T :

$$T = (\text{Number of cells} - 1) \times \text{cell size} = 115 \text{ mm}$$

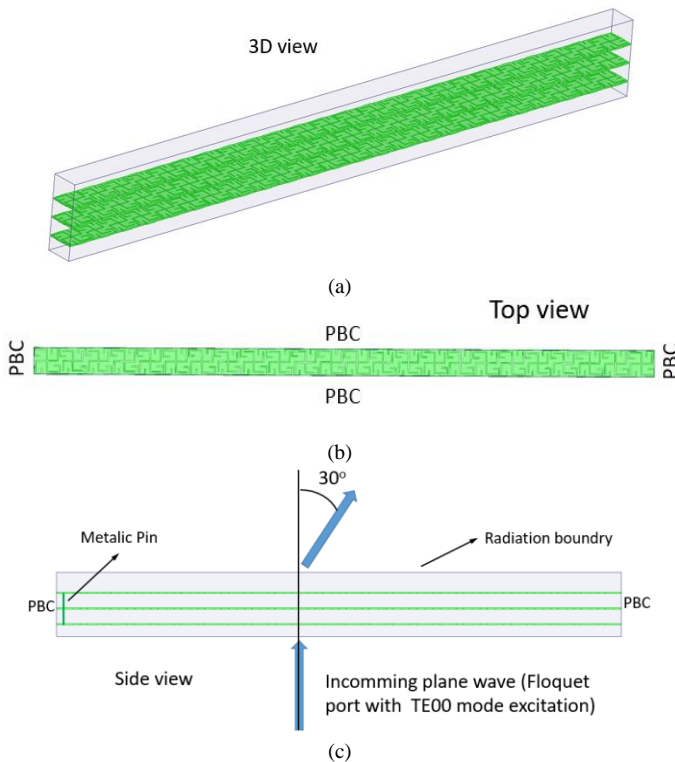


Fig. 14 - A schematic view of the simulated super cell: (a) 3D view; (b) top view; (c) excitation and deflection process.

Thus, periodic boundary condition can also be applied to the array extremities which in turn constitutes a super cell (see Fig. 14b).

In Fig. 15, simulation results of HFSS are compared with those obtained by theory where each cell is considered as an individual omnidirectional radiator (phased-array theory) with its specific amplitude and phase. As shown, there is a good agreement between the two methods. The array shows overall gain of 10.3 and 12.7 dB at 20 and 30 GHz. In practice, the performance will be improved by gold plating the stainless steel and optimizing the relative distance between the layers. These results are quite promising for future applications, especially those intended for space communication systems.

VI. SUMMARY AND CONCLUSIONS

In this paper, we have introduced a cell topology for a transmitarray antenna demonstrating a dual-band, dual-polarized operation at 20 and 30 GHz. Independent performance at each frequency, simplicity of design and the potential to be implemented as a fully metallic transmitarray are among the advantages of the new cell compared with similar prototypes introduced so far. As a proof-of-concept, a small transmitarray fed by a dual-band circularly polarized feed was fabricated and measured wherein, beam steering was accomplished by a relative translational displacement of the transmitarray respect to the feeder. The measured results, confirmed by simulations carried out with CST, HFSS and FEKO, reveal the large potentialities of the new design for future satellite applications, both on earth and in space, especially with larger transmitarray surfaces and specially tailored feeders. Moreover, the presented performances can be

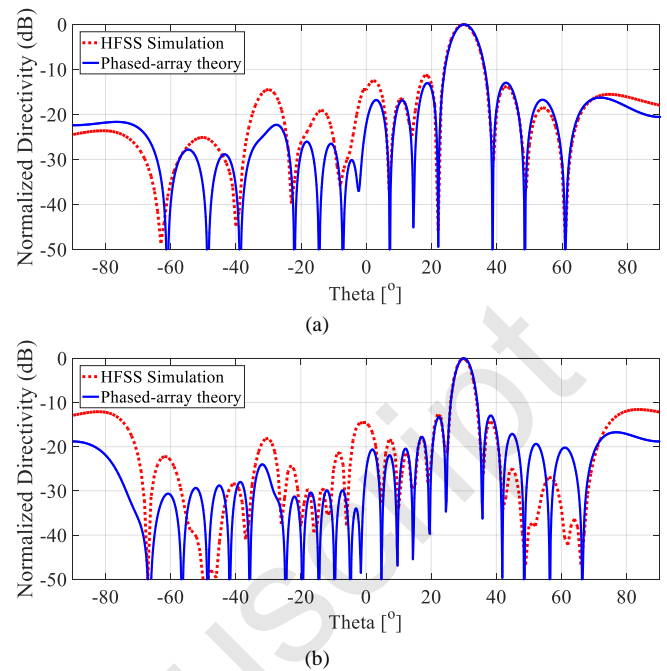


Fig. 15 - Comparison of simulation results obtained with HFSS (red curve) with that of theory, computed with MATLAB (blue): (a) at 20 GHz; (b) at 30 GHz.

improved by optimizing the layers' separation, increasing their number and, in the case of a fully metallic transmitarray, gold plating the stainless-steel parts.

REFERENCES

- [1] Newsat, "Ka-band," Sep. 2012 [Online]. Available: <http://www.newsat.com/whitepapers/572-ka-band-white-paper/file>, accessed on Oct. 2016.
- [2] King-Wai Lam, Sze-Wai Kwok, Yeongming Hwang and T. K. Lo, "Implementation of transmitarray antenna concept by using aperture-coupled microstrip patches," *Proceedings of 1997 Asia-Pacific Microwave Conference*, 1997, pp. 433-436 vol.1
- [3] M. R. Chaharmir, A. Ittipiboon and J. Shaker, "Single-band and dual-band multilayer transmitarray antennas," *2006 12th International Symposium on Antenna Technology and Applied Electromagnetics and Canadian Radio Sciences Conference*, Montreal, QC, Canada, 2006, pp. 1-4.
- [4] T. Chaloun, C. Hillebrand, C. Waldschmidt and W. Menzel, "Active transmitarray submodule for K/Ka Band Satcom applications," *2015 German Microwave Conference*, Nuremberg, 2015, pp. 198-201.
- [5] S. Zainud-Deen, S. M. Gaber, H. Malhat and K. H. Awadalla, "B2. Single Feed Dual-Polarization Dual-Band Transmitarray for Satellite Applications," *2013 30th National Radio Science Conference (NRSC)*, Cairo, Egypt, 2013, pp. 27-34.
- [6] H. Hasani, J. S. Silva, J. R. Mosig and M. Garcia-Vigueras, "Dual-band 20/30 GHz circularly polarized transmitarray for SOTM applications," *2016 10th European Conference on Antennas and Propagation (EuCAP)*, Davos, 2016, pp. 1-3.
- [7] P. Naseri, R. Mirzavand and P. Mousavi, "Dual-band circularly polarized transmit-array unit-cell at X and K bands," *2016 10th European Conference on Antennas and Propagation (EuCAP)*, Davos, 2016, pp. 1-4.
- [8] M. O. Bagheri, H. R. Hassani and B. Rahmati, "Dual-band, dual-polarised metallic slot transmitarray antenna," in *IET Microwaves, Antennas & Propagation*, vol. 11, no. 3, pp. 402-409, 19 2 2017.
- [9] S. A. Matos *et al.*, "High Gain Dual-Band Beam-Steering Transmit Array for Satcom Terminals at Ka-Band," in *IEEE Transactions on Antennas and Propagation*, vol. 65, no. 7, pp. 3528-3539, July 2017.
- [10] E. B. Lima, S. A. Matos, J. R. Costa, C. A. Fernandes and N. J. G. Fonseca, "Circular Polarization Wide-Angle Beam Steering at Ka-Band by In-Plane Translation of a Plate Lens Antenna," in *IEEE Transactions*

- on *Antennas and Propagation*, vol. 63, no. 12, pp. 5443-5455, Dec. 2015.
- [11] K. Pham, R. Sauleau, E. Fourn, F. Diaby, A. Clemente and L. Dussopt, "Dual-band dual-polarized transmitarrays at Ka-band," 2017 11th European Conference on Antennas and Propagation (EUCAP), Paris, 2017, pp. 59-62.
- [12] J. Perruisseau-Carrier, "Optimal Cell Topology Constraint for Monolayer Dual-Polarized Beamscanning Reflectarrays," in *IEEE Antennas and Wireless Propagation Letters*, vol. 11, pp. 434-437, 2012.
- [13] A. H. Abdelrahman, A. Z. Elsherbeni and F. Yang, "Transmission Phase Limit of Multilayer Frequency-Selective Surfaces for Transmitarray Designs," in *IEEE Transactions on Antennas and Propagation*, vol. 62, no. 2, pp. 690-697, Feb. 2014.
- [14] <https://www.cst.com/>
- [15] <https://www.feko.info/>
- [16] J. S. Silva; M. García-Viguera; T. Debogović; J. R. Costa; C. A. Fernandes; J. R. Mosig, "Stereolithography-Based Antennas for Satellite Communications in Ka-Band," in *Proceedings of the IEEE*, vol.105, no.04, pp.655-667, Mar. 2017.
- [17] J. S. Silva, M. García-Viguera, T. Debogovic and J. R. Mosig, "3D-printed Ka-band antenna based on stereolithography," 2017 11th European Conference on Antennas and Propagation (EUCAP), Paris, 2017, pp. 589-593.
- [18] <http://www.ansys.com/>